Resonant Microwave Power Absorption in Slabs and Cylinders

K. G. Ayappa
Dept. of Chemical Engineering, Indian Institute of Science, Bangalore, India 560012

H. T. Davis
Dept. of Chemical Engineering and Materials Science, University of Minnesota, Minneapolis, MN 55455

S. A. Barringer and E. A. Davis
Dept. of Food Science and Nutrition, University of Minnesota, St. Paul, MN 55108

Resonant power absorption is an important phenomenon during microwave heating. The resonances that occur when plane electromagnetic waves are incident on infinitely long cylinders and slabs are investigated as a function of sample dimensions. For cylinders two kinds of incident waves are studied: TM^z *when the electric field is oriented along the axis of the cylinder and* TE^z *when the magnetic field is oriented along the axis. At a resonant condition the average power absorbed by the sample is a local maximum. Due to attenuation within the sample the resonances decrease in intensity as the sample size increases. Using the dielectric properties of water, resonances are found to be a function of the ratio of the sample dimension to the wavelength of radiation,* λ_s*, in the sample. For slabs of thickness L and integer values of n, resonances occurred at* $L/\lambda_s = 0.5n$*; for cylinders of diameter D, resonances occurred at* $D/\lambda_s = 0.5n - 0.257$*. The generality of these relations to predict resonances in other food samples are shown using existing dielectric data. Resonances in cylinders for both polarizations occurred at similar radii. However, the radius at which the first resonance occurred for the* TM^z *case was absent in the* TE^z *case.*

Introduction

In microwave heating applications the amount of power absorbed by the sample is dependent upon the frequency and intensity of incident radiation. At a fixed frequency and intensity of the incident microwaves, the amount of power absorbed is determined by the geometry and dielectric properties of the sample. The spatial distribution of absorbed power is deduced by solving Maxwell's equations, and the temperature rise in the sample is obtained by an appropriate energy balance.

In a recent study by Barringer et al. (1994) heating rates of cylindrical samples of oil and water were compared. The experiments were conducted in a commercial domestic oven and in a customized oven built with a unidirectional microwave source to mimic plane waves. An important feature of this study was the resonant heating behavior that was observed in the customized oven when the radius of the cylinder was varied. At a resonant condition the power absorbed by the sample increases sharply. The resonances occurred with decreasing intensity as the sample radius was increased, and the heating rate was found to increase significantly during a resonance. The cylinder radii at which these resonant heating conditions were observed in the customized oven were in excellent agreement with those predicted by solving Maxwell's equations for a plane-wave incident on an infinitely long cylindrical sample.

Ohlsson and Risman (1978) have conducted microwave heating experiments at 2,450 MHz on spherical and cylindrical samples. Pronounced heating in the center of the object was observed for spheres and cylinders with diameters in the ranges of 2–6 cm and 1.8–3.5 cm, respectively. During hyperthermia, where the human body is exposed to low-intensity

Correspondence concerning this article should be addressed to K. G. Ayappa.
Present address of S. A. Barringer: Department of Food Science and Technology, The Ohio State University, 122 Vivian Hall, 2121 Fyffe Road, Columbus, OH 43210.

radiation, frequencies at which resonances occur must be avoided. Much of the early work on resonant power absorption studied the effect of electromagnetic absorption in cylindrical and spherical models of man. Massoudi et al. (1979a,b) studied the average power absorbed in homogeneous and multilayered cylindrical models by varying the frequency of radiation for a sample with fixed diameter. Average powers were calculated for frequencies in the 20–10,000 MHz range. The frequency dependence of the dielectric properties of materials used in their study were not reported. Their calculations showed the presence of resonances only in the multilayered samples. Ruppin (1979) studied the average power absorption for cylinders in the presence of a reflecting surface in the 10–10,000 MHz frequency range. The dielectric properties were assumed to be frequency dependent; however, in this frequency range no significant resonances were observed in the absence of the reflecting surface.

Resonant power absorption in spheres is more pronounced and has received greater attention. Weil (1975) predicted the average power absorbed in spheres over the frequency range 100–10,000 MHz. Dielectric data were assumed to vary with frequency and were collected from a variety of sources in the literature. Calculations for spheres of radius 3.3 cm and 6 cm show strong resonances when the frequency is varied. Other studies on the absorption of power in spheres are those by Kritikos and Schwan (1972), Lin et al. (1973), Shapiro et al. (1971), Jones and Spiegel (1974), Morgan (1981), and Tuntomo et al. (1991).

Resonant power absorption can cause superheating in liquid systems. This phenomenon has been used in the design of cylindrical reaction vessels to take advantage of the higher reaction rates due to the increase in temperature (Michael et al., 1991). Pangrle et al. (1991), while studying thawing of cylindrical samples exposed to a radially symmetric microwave field, observed sharp increases in the front velocity due to resonant power absorption. The enhanced heating rate during a resonant condition may lead to runaway effects. To effectively design and control microwave-related processes it is useful to have a knowledge of when resonant power absorption occurs.

Though the literature on electromagnetic scattering and absorption with cylinders is quite extensive, a systematic study of the resonance phenomenon as observed by Barringer et al. (1994) has not been reported. Fu and Metaxas (1992) observed an oscillatory behavior in the power-absorption coefficient in slabs. Resonant power absorption in slabs has received very little attention in the literature.

Using the dielectric properties of water over the frequency range 1,100–57,000 MHz we systematically investigated resonances that occur in cylindrical and slab-like samples exposed to plane waves. In the case of the cylinder, two kinds of incident-wave polarizations were studied. When the incident electric field is along the axis of the cylinder, it is referred to as the TM^z polarization, and when the electric field is perpendicular to the axis, it is referred to as TE^z polarized. The electric field and power distributions for both polarizations are derived from analytical solutions of Maxwell's equations. Resonances are found to be systematic, and linear relations that can be used to predict these resonances are obtained. The generality of the relations to predict resonances in other cylindrical and slab-shaped samples of food materials is illustrated using dielectric properties tabulated in the literature.

Theory

Maxwell's equations govern the propagation of electromagnetic radiation. By solving Maxwell's equations the spatial variation of the electric field, $\boldsymbol{E}$, within the sample is obtained and the volumetric power absorbed is

$$P(\boldsymbol{r}) = \frac{1}{2}\omega\epsilon_0\kappa''\boldsymbol{E}\cdot\boldsymbol{E}^*, \tag{1}$$

where ϵ_0 is the free-space dielectric constant and $\omega = 2\pi f$, where f is the frequency of radiation and κ'' is the relative dielectric loss of the sample. In Eq. 1, $\boldsymbol{E}^*$ is the complex conjugate of $\boldsymbol{E}$. The spatially varying microwave power from Eq. 1 is averaged to predict the average power $\bar{P}$ absorbed by the sample

$$\bar{P} = \frac{\int_\Omega P(\boldsymbol{r})d\boldsymbol{r}}{\int_\Omega d\boldsymbol{r}}, \tag{2}$$

where Ω represents integrations over the volume of the sample. Local maxima in the plot of average power vs. sample radius for cylinders, and sample thickness for slabs, indicate the dimensions at which a resonance occurs.

The wavelength within the sample λ_s, and the penetration depth D_p, influence the absorption of power during microwave heating. They are both functions of the relative dielectric constant κ', and the relative dielectric loss κ'', of the material. The wavelength of radiation, λ_s, in the sample is

$$\lambda_s = \frac{\lambda_0}{\sqrt{\frac{\kappa'}{2}}\sqrt{\sqrt{1+\left(\frac{\kappa''}{\kappa'}\right)^2}+1}}. \tag{3}$$

The penetration depth, D_p, or distance at which the incident electric field has decayed to $1/e$ of its incident value, is

$$D_p = \frac{\lambda_0}{\pi\sqrt{2\kappa'}\sqrt{\sqrt{1+\left(\frac{\kappa''}{\kappa'}\right)^2}-1}}. \tag{4}$$

Two incident plane-wave configurations on the infinite cylinders as illustrated in Figure 1 have been studied.

Cylinder: TM^z polarization

In this case the incident electric field is oriented along the axis of the cylinder. The electric-field distribution in a cylinder of radius R, obtained by solving Maxwell's equations with a time dependence of the form $e^{-i\omega t}$ (Ayappa et al., 1992; Balanis, 1989), is

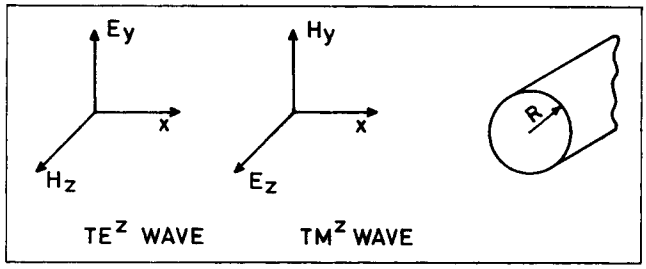

Figure 1. Two kinds of incident wave polarizations.

When the incident wave has its electric-field vector oriented along the cylinder axis, the polarization is referred to as TM^z polarization, and when the electric field is perpendicular to the axis, it is referred to as TE^z polarization.

$$E_z(r,\phi) = \sum_{n=0}^{\infty} a_n J_n(kr)\cos n\phi, \qquad 0 \le r \le R, \tag{5}$$

where the coefficients

$$a_n = E_0 \epsilon_n i^n \left[\frac{J_n'(k_0R)H_n^{(1)}(k_0R) - J_n(k_0R)H_n^{(1)'}(k_0R)}{\sqrt{\kappa^*}J_n'(kR)H_n^{(1)}(k_0R) - J_n(kR)H_n^{(1)'}(k_0R)} \right] \tag{6}$$

and

$$\epsilon_n = \begin{cases} 1, & n = 0; \\ 2, & \text{otherwise.} \end{cases}$$

$\kappa^* = \kappa' + i\kappa''$ is the relative complex permittivity, $H_n^{(1)}$ is the Hankel function of the first kind, and J_n is the nth-order Bessel function of the first kind (Abramowitz and Stegun, 1970). In the preceding equations, $i = \sqrt{-1}$ and the magnetic permeability of the sample is assumed to be that of free space. In Eq. 6, the propagation constant in free space

$$k_0 = (2\pi/\lambda_0), \tag{7}$$

and the propagation constant in the sample

$$k = (2\pi/\lambda_0)\sqrt{\kappa' + i\kappa''}. \tag{8}$$

Using the dimensionless variables

$$u = \frac{E}{E_0}, \qquad \rho = \frac{r}{R}, \qquad P_c = \frac{2\bar{P}}{E_0^2 \omega \kappa'' \epsilon_0}, \qquad \text{and} \qquad \gamma = kR, \tag{9}$$

the expression for dimensionless average power in the cylinder for transverse magnetic polarization is

$$P_c^{tm} = \frac{1}{\pi}\int_{\rho=0}^{1}\int_{\phi=0}^{2\pi} uu^* \rho \, d\rho \, d\phi. \tag{10}$$

Substituting the expression for the electric field in Eq. 10, and using the orthogonality of $\cos n\phi$; $0 \le \phi \le 2\pi$, the resulting expression for the average power is

$$P_c^{tm} = \sum_{n=0}^{\infty} \delta_n b_n I_{n,n}, \tag{11}$$

where

$$\delta_n = \begin{cases} 2, & n = 0; \\ 1, & \text{otherwise,} \end{cases} \qquad b_n = \frac{|a_n|^2}{E_0^2},$$

and

$$I_{n,n} = \int_0^1 \rho J_n(\gamma\rho)J_n(\gamma^*\rho)\,d\rho = \frac{1}{\gamma^2 - \gamma^{*2}}[\gamma J_n(\gamma^*)J_{n+1}(\gamma) - \gamma^* J_n(\gamma)J_{n+1}(\gamma^*)], \tag{12}$$

γ^* is the complex conjugate of γ, and $|a_n|$ denotes the modulus of a_n. The integral in Eq. 12, which involves the product of two Bessel functions, is known as the Lommel integral (McLachlan, 1934; Watson, 1966). Details of the derivation for Eq. 11 are given in the Appendix. Given the dielectric properties of a material at a particular frequency, Eq. 11 can be used to obtain the average power absorbed in cylinders as a function of R.

Cylinder: TE^z polarization

The solution for the TE^z polarized wave consists of first obtaining the solution for the magnetic field in the sample. The magnetic field induced in the cylinder of radius R is

$$H_z(r,\phi) = \sum_{n=0}^{\infty} c_n J_n(kr)\cos n\phi. \qquad 0 \le r \le R, \tag{13}$$

where

$$c_n = H_0 \epsilon_n i^n \left[\frac{J_n'(k_0R)H_n^{(1)}(k_0R) - J_n(k_0R)H_n^{(1)'}(k_0R)}{\sqrt{1/\kappa^*}J_n'(kR)H_n^{(1)}(k_0R) - J_n(kR)H_n^{(1)'}(k_0R)} \right] \tag{14}$$

and

$$\epsilon_n = \begin{cases} 1, & n = 0; \\ 2, & \text{otherwise.} \end{cases}$$

With a knowledge of the magnetic field the electric-field components are deduced from

$$E_\phi = \frac{1}{i\omega\epsilon_0\kappa^*}\frac{\partial H_z}{\partial r} \tag{15}$$

and

$$E_r = \frac{-1}{ir\omega\epsilon_0\kappa^*}\frac{\partial H_z}{\partial\phi}. \tag{16}$$

Using the dimensionless variables

$$u_\phi = \frac{E_\phi}{E_0} \quad \text{and} \quad u_\rho = \frac{E_\rho}{E_0},$$

the expression for the dimensionless average power in the cylinder for the TE^z polarization is

$$P_c^{te} = \frac{1}{\pi}\int_{\rho=0}^{1}\int_{\phi=0}^{2\pi}[u_\phi u_\phi^* + u_\rho u_\rho^*]\,\rho\,d\rho\,d\phi. \tag{17}$$

Inserting the expressions for u_ϕ and u_ρ from Eqs. 15 and 16 into Eq. 17, we get

$$P_c^{te} = 2d_0 I_{1,1} + \frac{1}{2}\sum_{n=1}^{\infty} d_n[I_{n+1,n+1} + I_{n-1,n-1}], \tag{18}$$

where

$$d_n = \frac{|c_n|^2}{H_0^2\sqrt{\kappa'^2 + \kappa''^2}} \qquad n = 0, \ldots, \infty.$$

In the preceding equations $|c_n|$ is the modulus of c_n and the integrals $I_{n,n}$ are given in Eq. 12. The derivation of Eq. 18, which is a little more detailed than that of Eq. 11, is given in the Appendix.

Slab

The expression for the power absorbed by a slab of thickness L exposed to a plane wave, which was derived in an earlier work on microwave heating of slabs (Ayappa et al., 1991), is

$$P(z) = \frac{1}{2}\omega\epsilon_0\kappa'' E_0^2 T^2\left[\frac{e^{-2\beta z} - 2Re^{-2\beta L}\cos[\delta + 2\alpha(L-z)] + R^2 e^{-2\beta L}e^{-2\beta(L-z)}}{1 - 2R^2e^{-2\beta L}\cos(2\delta + 2\alpha L) + R^4 e^{-4\beta L}}\right] \tag{19}$$

$$0 \le z \le L,$$

where

$$T = \sqrt{\frac{4\alpha_0^2}{(\alpha_0+\alpha)^2 + \beta^2}} \tag{20}$$

$$R = \sqrt{\frac{(\alpha_0-\alpha)^2 + \beta^2}{(\alpha_0+\alpha)^2 + \beta^2}} \tag{21}$$

and

$$\delta = \tan^{-1}\left[\frac{2\alpha_0\beta}{(\alpha^2 + \beta^2 - \alpha_0^2)}\right]. \tag{22}$$

R and δ are the modulus and the phase angle of the reflection coefficient, and T is the modulus of the transmission coefficient. In Eqs. 20, 21, and 22, α, the phase factor and β, the attenuation factor in the sample, are related to the penetration depth D_p and wavelength λ_s by

$$D_p = \frac{1}{\beta} \quad \text{and} \quad \lambda_s = \frac{2\pi}{\alpha}, \tag{23}$$

and in free space $\lambda_0 = 2\pi/\alpha_0$. Using the dimensionless variables $x = z/L$, the expression for the dimensionless average power in the slab is

$$\bar{P}_s = \int_0^1 P(x)\,dx. \tag{24}$$

The integral in Eq. 24 can be evaluated analytically using the expression for power from Eq. 19.

Results and Discussion

Dielectric properties

Average power distributions as a function of the cylinder radius R, and slab thickness L, were calculated for water over the frequency range 1.1–57 GHz. All computations for the average power were carried out for an incident plane-wave intensity I_0 of 3 $W\cdot cm^{-2}$. The incident electric field E_0 is related to I_0 by the following relationship:

$$E_0 = \sqrt{\frac{2I_0}{c\epsilon_0}}. \tag{25}$$

The average power as a function of sample radius for the TM^z polarization was calculated using Eq. 11. The accuracy of the average power computed with the series expression was checked by direct integration of Eq. 10. The integrations were performed using finite-element biquadratic basis functions on a 144-element mesh. The values of the average powers obtained by both methods were in excellent agreement. Typically about 15–20 terms were used to evaluate the series in Eqs. 11. For the TE^z polarizations the power was calculated using Eq. 17. Since all our results were based on calculations for TM^z polarization, Eq. 18 was not evaluated.

The dielectric properties of water have been tabulated for frequencies ranging from 1.1 to 57 GHz and temperatures varying from 273.15 to 323.15 K by Kaatze (1989), who fit the data to a Debye model of the form

$$\kappa' + i\kappa'' = \kappa_\infty + \frac{\kappa_0 - \kappa_\infty}{1 - i\omega\tau}, \tag{26}$$

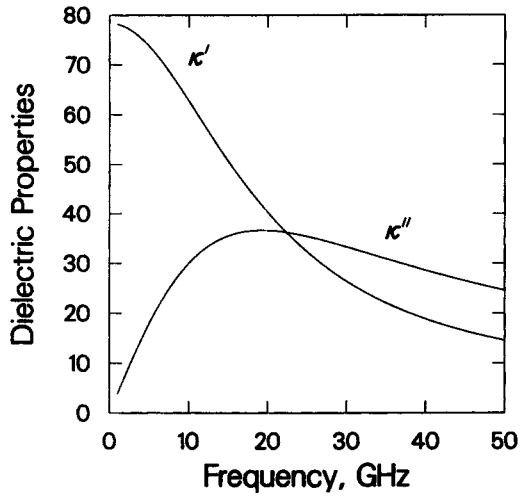

Figure 2. Relative dielectric loss κ'' and relative dielectric constant κ' of water as a function of frequency, predicted by the correlation from Kaatze (1989), Eq. 26.

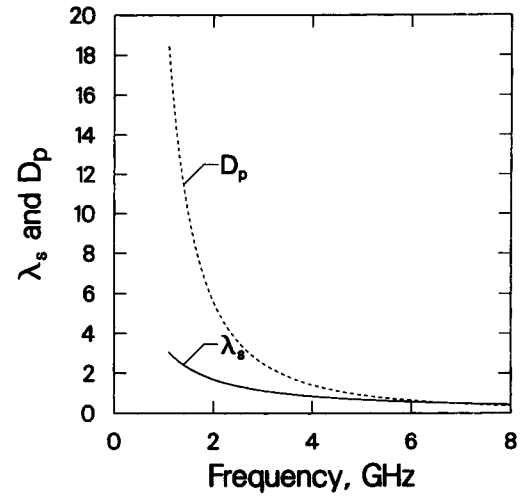

Figure 3. Wavelength λ_s, and penetration depth D_p, for water as a function of frequency calculated from the dielectric data of Kaatze (1989) for water.

At low frequencies the D_p is much larger than λ_s. However, above 7 GHz their magnitudes are comparable, with λ_s being slightly larger than D_p.

where the static dielectric constant,

$$\kappa_0 = 10^{1.94404 - 1.991 \times 10^{-3}(T - 273.15)},$$

the optical dielectric constant,

$$\kappa_\infty = 5.77 - 2.74 \times 10^{-2}(T - 273.15),$$

and the relaxation time constant is

$$\tau = 3.745 \times 10^{-15} s[1 + (7 \times 10^{-5}) \times (T - 300.65)^2] \exp(2.2957 \times 10^3 / T).$$

In the preceding expression T is the temperature in kelvins. Expressions for the dielectric constant and dielectric loss are obtained by equating real and imaginary parts of Eq. 26.

Figure 2 illustrates the dielectric constant κ' and the dielectric loss κ'' at 298 K as a function of frequency, as predicted by Eq. 26. Using Eqs. 3 and 4, the wavelength, λ_s, and penetration depth, D_p, were calculated as a function of frequency, and are plotted as shown in Figure 3. Both λ_s and D_p decrease with increasing frequency. At low frequencies D_p is significantly larger than λ_s.

Resonances in cylinders and slabs

Figure 4a illustrates the average power as a function of R/λ_s for TM^z and TE^z polarizations for water at $f = 2{,}450$ MHz. At this frequency $\kappa' = 77.22$, $\kappa'' = 9.18$ and $\lambda_s = 1.39$ cm and the penetration depth $D_p = 3.73$ cm. The average power for the TM^z case is much greater than the TE^z case, indicating that the coupling is more effective when the electric field is oriented along the sample axis. The difference in the average power is greater for cylinders with small radii, and in the large cylinders the average power is independent of the polarization of the incident wave. The local maxima in the average power indicate cylinder radii at which resonant power absorption occurs. At these radii the waves within the sample interfere constructively, increasing the power absorption. At cylinder radii between two power maxima the interior field interacts destructively, giving rise to a minimum in the average power absorbed. Reflections off the back face weaken as the sample diameter increases and resonances decrease in intensity.

At smaller radii the average power for the TM^z case approaches a constant value. However, for the TE^z case the first resonance occurs at a radius corresponding to the radius at which the second resonance occurs for the TM^z case. As the sample radius decreases for the TM^z polarization, the absorbed power shows little spatial variation, and below the sample radius at which the first resonant peak occurs, the power in the sample reduces to a constant as the radius is further decreased. The limiting value of the absorbed power as the radius approaches zero can be examined by using the asymptotic forms of the special functions (Abramowitz and Stegun, 1970) in the expression for the electric field given by Eq. 5. As the sample radius decreases, the asymptotic value of the induced electric field approaches the incident field strength E_0, and the power absorbed by the sample reduces to the constant value

$$P = \frac{1}{2}\omega\epsilon_0\kappa'' E_0^2. \tag{27}$$

The value of the power calculated using Eq. 11, for small radii, agreed very well with the power deduced from the asymptotic limit, Eq. 27.

Equations 14, 15 and 16 for the TE^z polarization, show that the magnetic field behaves in a qualitatively similar manner to the electric field in the TM^z case. Since the electric field in the TE^z polarization is obtained by taking derivatives

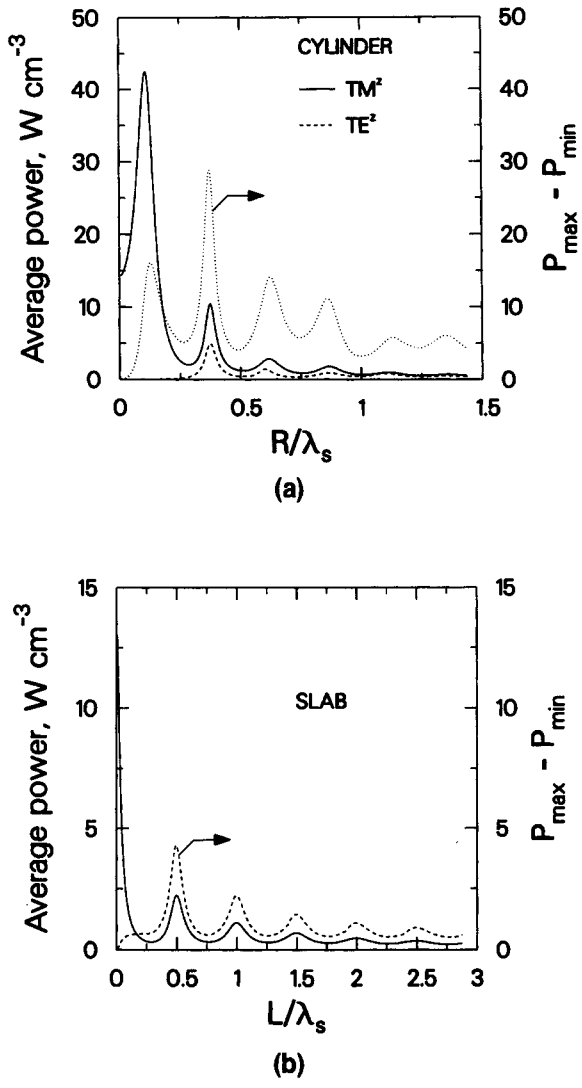

Figure 4. (a) Comparison of average power absorption for the TM^z and TE^z polarizations; (b) average power for slabs.

The frequency of radiation $f = 2{,}450$ MHz, $\lambda_s = 1.39$ cm, $D_p = 3.73$ cm, $\kappa' = 77.22$, and $\kappa'' = 9.18$. With the exception of the first resonant condition, the R/λ_s ratios at which resonances occur are identical in both samples. The average power absorbed for the TM^z case is much higher for the smaller samples. The difference between the maximum and minimum power plotted for the TM^z case illustrates that the power distribution is most nonuniform when a resonance occurs.

of the magnetic field, the constant value of the induced magnetic field at smaller radii causes the electric field and hence the power to tend to zero.

In most microwave heating applications it is desirable to maintain a uniform temperature in the sample. The uniformity of sample temperature is dependent on the spatial distribution of power. To assess the extent of the spatial variation of power in the sample, the difference between the maximum and minimum power, $P_{max} - P_{min}$, in the sample at a given radius is also plotted in Figure 4a. The greatest spatial variation in power is seen to occur at the second resonance. The maxima in $P_{max} - P_{min}$ occur at identically the same radii at which these resonances occur. Thus during a resonance, in addition to the sample heating at a higher rate, the nonuniformity in heating is also accentuated.

Also of interest is the spatial distribution of power during a resonance. For the first and third resonances the maximum power peak is located at the center of the cylinder with the maximum in the center being very pronounced for the third resonance. At other resonances no systematic behavior in the power maximum was observed. Ohlsson and Risman (1978) in an experimental study of microwave heating in a commercial oven (34×31.2×30.8 cm) observed that center heating was predominant for cylinder diameters between 2.0 and 3.5 cm. Using the dielectric properties of the phantom food used in their study, the third and fourth resonance predicted by Eq. 11 occurred at diameters 2.1 and 2.9 cm. Ohlsson and Risman (1978) report that at a diameter of 2.5 cm the heating at the center was most pronounced. This appears to be consistent with our observation that at the third resonance the power deposited in the center is a maximum; however, the diameter at which the resonance occurs can only be estimated from the plane-wave model developed here.

In a recent work (Barringer et al., 1994) we have compared the heating rates of cylindrical samples of water and observed the presence of resonant heating conditions depending on the radius of the sample. The experiments were carried out in a customized oven built to mimic a plane-wave configuration. The radii at which resonances occurred were accurately predicted using the average power distributions for the TM^z polarized wave. In similar experiments carried out in a domestic oven, resonances were not observed (Barringer et al., 1994) and heating rates simply decreased with increased radius. In addition to the complex standing-wave patterns produced within the oven, the location of the sample within the oven influences the power absorption. Resonances predicted using plane waves give an estimate of a possible resonance situation that might occur in an oven. In general the plane-wave model must be used with caution while trying to predict resonances in a cavity.

Figure 4b illustrates the average power vs. L/λ_s, for $f =$ 2,450 MHz. Here again the average power is oscillatory, giving rise to resonances. For thin slabs the power absorption is seen to rise to a maximum value. The values of $P_{max} - P_{min}$ illustrate that the power is uniform in thin slabs and is most nonuniform during a resonance. Fu and Metaxas (1992) have observed the oscillatory behavior in the absorption coefficient (which is related to the total power absorbed) of slabs. Unlike in the case of the cylinders, the power profiles for the slabs show no pronounced heating in the center.

Relations for resonances

In Figure 5a the dimensionless average power for the TM^z polarization is plotted against R/λ_s for three different frequencies. The resonances are seen to occur at fixed R/λ_s ratios. A similar plot for slabs is shown in Figure 5b, where resonances occur at fixed L/λ_s ratios.

The R/λ_s and L/λ_s ratios were calculated from plots similar to Figures 4a and 4b, for frequencies ranging from 1,100 to 5,700 MHz, in the following manner. In this frequency range the wavelength of radiation in the sample varies from 0.61 cm at 5,700 MHz to 3.08 cm at 1,100 MHz. For each plot of average power vs. sample radius, corresponding to a par-

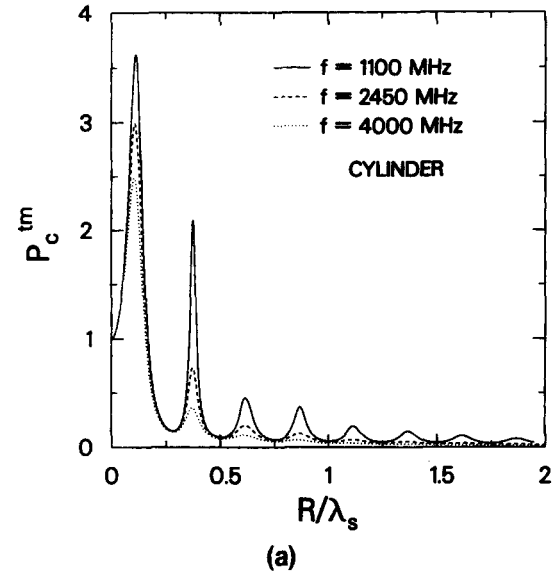

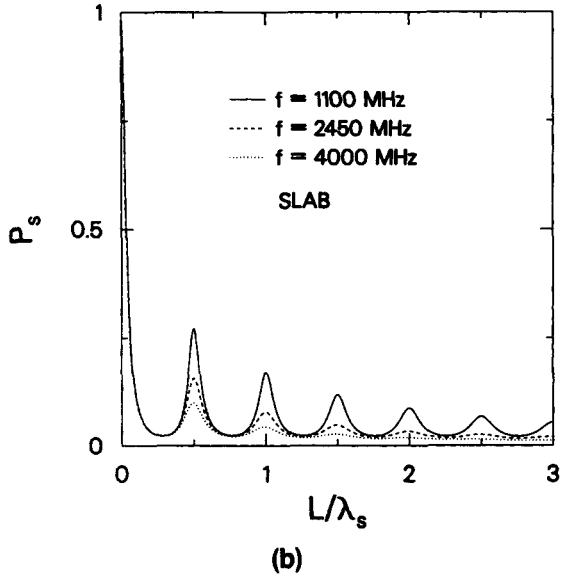

Figure 5. Dimensionless average powers for the cylinder and slab plotted against (a) R/λ_s and (b) L/λ_s ratios for three different frequencies.

Resonances are seen to occur at a fixed sample dimension-to-wavelength ratio.

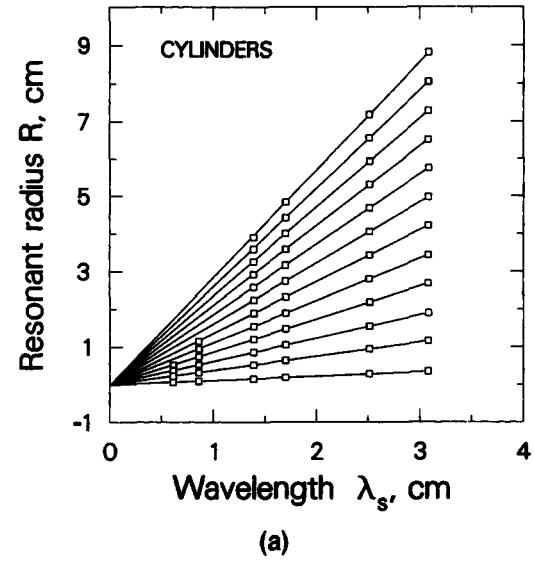

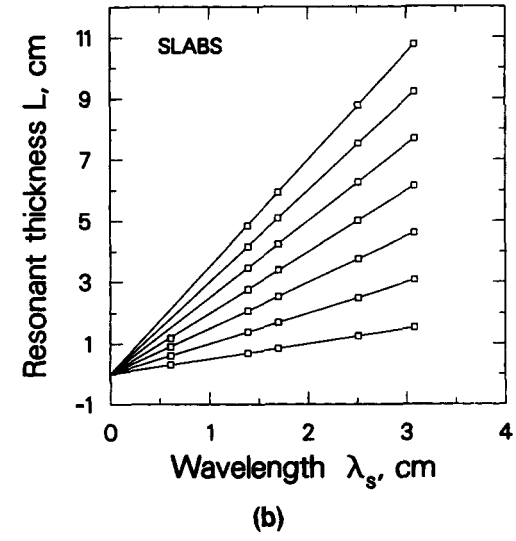

Figure 6. (a) Cylinder radii R at which resonances occur are plotted vs. λ_s; (b) data plotted for slabs.

In (a) each resonant peak is seen to occur at a fixed R/λ_s ratio. As the wavelength increases, the resonances occur at larger radii, and as the wavelength approaches zero all the lines extrapolate back to the origin, indicating that no resonances are observed. For small values of λ_s corresponding to higher frequencies the penetration depths are smaller than the wavelengths (Figure 3) and fewer resonances are observed. In (b) the resonances in slabs are much weaker than in cylinders, and slab thicknesses up to 7 resonances are shown.

ticular value of λ_s, the radii at which resonances occurred were located numerically using a simple finite-difference slope criterion and plotted against the wavelength λ_s as illustrated in Figure 6a. In Figure 6a, the cylinder radii at which resonances occur at a fixed λ_s are plotted along the y-axis. As λ_s in the sample increases, resonances occur at larger radii. The resonant cylinder radii were calculated for the TM^z polarization. In the case of the TE^z polarization the first resonance was absent but all other resonances occurred at identical radii, as shown in Figure 4a. All the lines extrapolate back to the origin, illustrating that as the wavelength approaches zero, resonances no longer exist. As the frequency increases, the penetration depth decreases rapidly, as seen in Figure 3, and the number of resonances observed are fewer.

The data for slabs were obtained using a similar procedure and are illustrated in Figure 6b. From Figures 6a and 6b the R/λ_s and L/λ_s ratios were computed by using linear fits to the data. Though Figures 6a and 6b can be used to find the dimension at which a particular resonance occurs when λ_s is known, a more concise relation is illustrated in Figure 7. The D/λ_s and L/λ_s ratios are plotted against the integer number n, corresponding to a particular resonance. For the first resonance, $n = 1$, 2 for the second, and so on. The linear least-squares fit obtained for the cylinders is

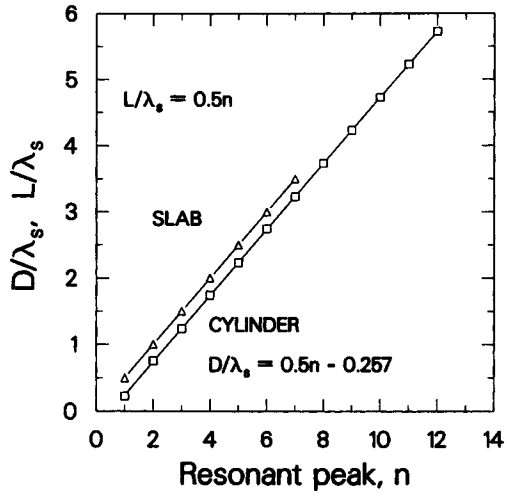

Figure 7. Linear relationship observed when D/λ_s ($D = 2R$), and L/λ_s ratios plotted against the integer number of the resonant peak.

$n = 1$ corresponds to the first peak, $n = 2$ to the second, and so on. Using this relationship, and the value of λ_s calculated from the dielectric properties, the sample dimensions at which a resonance occurs is easily determined.

$$\frac{D}{\lambda_s} = 0.5n - 0.257 \qquad (28)$$

$$n = 1, \ldots, 12,$$

where D is the diameter of the cylinder and the linear relation for slabs of thickness L is

$$\frac{L}{\lambda_s} = 0.5n, \qquad (29)$$

$$n = 1, \ldots, 7.$$

To avoid the presence of a physically unrealistic intercept, the data for Eq. 29 were fitted by constraining the fit to pass through the origin. The fit in the absence of the constraint yielded an intercept of 0.001. The resonances in the slab were weaker than the resonances in the cylinder and data for only seven resonances were obtained. From Eqs. 28 and 29, and a knowledge of λ_s, the cylinder diameter D and slab thickness L, at which a particular resonance occurs can easily be determined. $n = 1$ corresponds to the strongest resonance and $n = 12$ to the weakest.

Predicting resonances in food samples

Equations 28 and 29 were derived using the properties of water over the frequency range for which data were available. The applicability of the relations, Eqs. 28 and 29, to predict resonances in slabs and cylinders of other food materials was tested using dielectric properties tabulated in the literature. Using Eq. 3, λ_s was calculated and the resonances were located with the analytical expressions for average power, as was done earlier. In Figures 8a and 8b the radii at which resonances occurred in the samples are plotted vs. the sample dimensions predicted by Eqs. 28 and 29. The dielectric data and the wavelength of samples used are given in Table 1. Though the relation in Eqs. 28 and 29 was developed using the data for water in the wavelength range 0.61 to 3.08 cm and temperatures between 273.15 and 323.15 K, resonances in samples above this range appear to be predicted

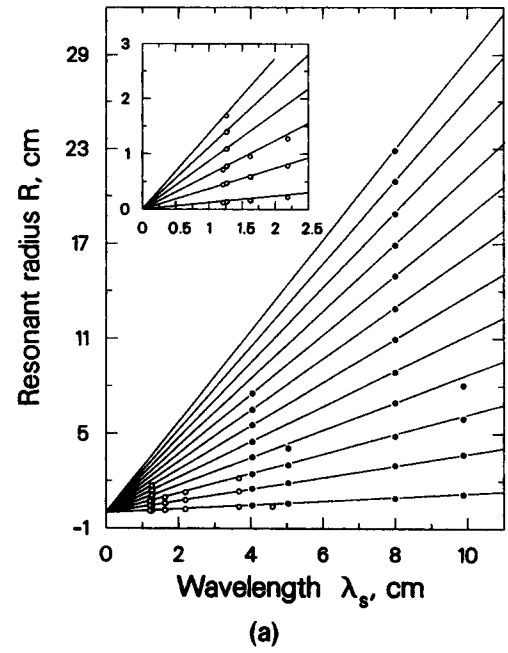

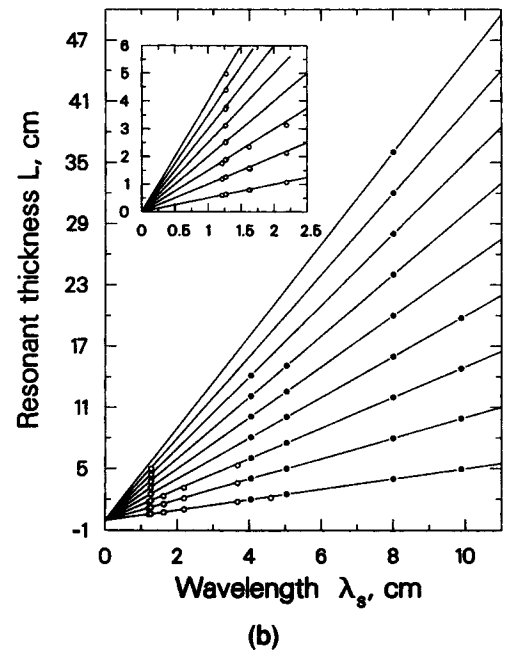

Figure 8. Cylinder radius (a) R and slab thickness (b) L at which resonances occur in a variety of food samples are plotted against λ_s.

The dielectric data of the samples that were used are given in Table 1. The symbols represent the resonant sample dimensions and the solid lines represent the resonant dimensions predicted by Eqs. 28 and 29. The shaded symbols represent data for water. It is seen that the relations derived using the dielectric properties of water can be used very effectively to estimate resonant dimensions in cylindrical and slab-shaped samples exposed to plane waves.

Table 1. Dielectric Data Used for Calculations in Figure 8

Sample	f (MHz)	κ'	κ''	λ_s
Beef cooked	2,450	30.5	9.6	2.19
0.1 M NaCl	2,800	71.1	13.7	1.26
Beef raw	2,800	42.6	13.1	1.62
Carrots cooked	2,800	70.1	11.8	1.27
Liver	2,800	41.4	16.5	1.63
Gravy	2,800	76.1	24.1	1.21
Potatoes raw	1,000	65.1	19.6	3.67
Beef raw	900	49.2	25.6	4.6
Water (313 K)	900	67.8	1.36	4.04
Water (413 K)	900	43.7	0.3	5.03
Water (313 K)	450	69.2	1.18	8.0
Water (413 K)	450	45.4	0.68	9.88

Data taken from Ohlsson and Bengtsson (1975).

quite well. Most of the dielectric data in the 2,450–2,800 MHz range correspond to wavelengths below 3.08 cm, and the data for samples in the 450–900-MHz region lie above 3.08 cm. The resonances for slab-like samples of water at 413 K and $\lambda_s = 5.03$ cm were predicted very well by Eq. 29; however, only the first four resonances were predicted accurately by Eq. 28 for the cylinders.

Conclusion

When a resonance occurs during microwave heating, the power absorbed rises sharply, giving rise to unusually large heating rates. To effectively develop, design and control microwave heating applications a prior knowledge of when these resonances occur is imperative. A systematic study of this phenomenon has not been reported in literature.

We have studied the conditions under which resonant power absorption occurs when slabs and cylindrical samples of water are exposed to plane waves. Our study illustrates that these resonances are only a function of sample dimension and wavelength of radiation in the sample. In the case of cylinders, resonances are independent of the polarization of the incident wave. With the absence of the first resonant peak for the TE^z polarization, all other resonances were observed to occur at identical cylinder radii for both polarizations. However, the intensity of the average power absorbed in smaller cylinders for the TE^z polarization was much lower than the TM^z case. At a resonant condition the difference between the maximum and minimum values of absorbed power also show local maxima. Hence at a resonance, not only is the heating rate increased but the uneven power distribution will accentuate the nonuniformity in heating.

At low frequencies the penetration depth of water is significantly higher than the wavelength of radiation in the sample, and a number of resonant conditions were observed. As the frequency increases the penetration depth decreases, and only a few resonances are observed.

Based on the properties of water, a linear relationship between sample diameter/thickness to wavelength, and the integer number of the resonance was found. With this simple relation and a knowledge of the dielectric properties of the sample, the sample dimensions at which a particular resonance occurs can easily be determined. Using the dielectric properties of a variety of food samples, the applicability of the relations to predict resonances in samples other than water is illustrated.

Acknowledgment

We thank the Supercomputer Education and Research Center, Indian Institute of Science, Bangalore, and the Minnesota Supercomputer Institute for computing resources, and Peter Foong for carrying out some of the preliminary computations.

Notation

E = electric field intensity, $V \cdot m^{-1}$
H = magnetic field intensity, $Amp \cdot m^{-1}$
P_c = dimensionless average volumetric power absorbed in cylinder
P_s = dimensionless average volumetric power absorbed in slab
μ_0 = free-space permeability, $H \cdot m^{-1}$
ω = angular frequency, $rad \cdot s^{-1}$

Subscripts and superscripts

c = cylinder
s = slab
tm = transverse magnetic
te = transverse electric

Literature Cited

Abramowitz, M., and I. A. Stegun, *Handbook of Mathematical Functions*, 9th ed., Dover, New York (1970).

Ayappa, K. G., H. T. Davis, E. A. Davis, and J. Gordon, "Two-Dimensional Finite Element Analysis of Microwave Heating," *AIChE J.*, **38**, 1577 (1992).

Ayappa, K. G., G. Crapiste, H. T. Davis, E. A. Davis, and J. Gordon, "Microwave Heating: An Evaluation of Power Formulations," *Chem. Eng. Sci.*, **46**, 1005 (1991).

Balanis, C. A., *Advanced Engineering Electromagnetics*, Wiley, New York (1989).

Barringer, S. A., E. A. Davis, J. Gordon, K. G. Ayappa, and H. T. Davis, "The Effect of Sample Size on Microwave Heating Rate: Comparison of Oil and Water," *AIChE J.*, **40**, 1433 (1994).

Fu, W., and A. Metaxas, "A Mathematical Derivation of Power Penetration Depth for Thin Lossy Materials," *J. Microwave Power*, **27**, 217 (1992).

Jones, W. T., and R. J. Spiegel, "Resonance Absorption of Microwaves by the Human Skull," *IEEE Trans. Biomed. Eng.*, **BME-21**, 46 (1974).

Kaatze, U., "Complex Permittivity of Water as a Function of Frequency and Temperature," *J. Chem. Eng. Data*, **34**, 371 (1989).

Kritikos, H. N., and H. P. Schwan, "Hot Spots Generated in Conducting Spheres by Electromagnetic Waves and Biological Implications," *IEEE Trans. Biomed. Eng.*, **BME-19**, 53 (1972).

Lin, C. L., A. W. Guy, and C. C. Johnson, "Power Deposition in a Spherical Model of Man Exposed to 1–20 MHz Electromagnetic Fields," *IEEE Trans. Microwave Theory Tech.*, **MTT-21**, 791 (1973).

Massoudi, H., C. H. Durney, and C. C. Johnson, "A Geometrical-Optics and an Exact Solution for Internal Fields in and Energy Absorption by a Cylindrical Model of Man Irradiated by an Electromagnetic Plane Wave," *Radio Sci.*, **14**, 35 (1979a).

Massoudi, H., C. H. Durney, P. W. Barber, and M. F. Iskander, "Electromagnetic Absorption in Multilayered Cylindrical Models of Man," *IEEE Trans. Microwave Theory Tech.*, **MTT-27**, 825 (1979b).

McLachlan, N. W., *Bessel Functions for Engineers*, Clarendon, Oxford, p. 94 (1934).

Michael, D., P. Mingos, and D. R. Baghurst, "Applications of Microwave Dielectric Heating Effects to Synthetic Problems in Chemistry," *Chem. Soc. Rev.*, **20**, 1 (1991).

Morgan, M. A., "Finite Element Calculation of Microwave Absorption by the Cranial Structure," *IEEE Trans. Biomed. Eng.*, **BME-28**, 687 (1981).

Ohlsson, T., and P. O. Risman, "Temperature Distribution of Microwave Heating-Spheres and Cylinders," *J. Microwave Power*, **13**, 303 (1978).

Ohlsson, T., and N. Bengtsson, "Dielectric Food Data for Microwave Sterilization," *J. Microwave Power*, **10**, 93 (1975).

Pangrle, B. J., K. G. Ayappa, H. T. Davis, E. A. Davis, and J. Gordon, "Microwave Thawing of Cylinders," *AIChE J.*, **37**, 1789 (1991).

Ruppin, R., "Electromagnetic Power Deposition in a Dielectric Cylinder in the Presence of a Reflecting Surface," *IEEE Trans. Microwave Theory Tech.*, **MTT-27**, 910 (1979).
Shapiro, A. R., R. F. Lutomirski, and H. T. Yura, "Induced Fields and Heating Within a Cranial Structure Irradiated by an Electromagnetic Plane Wave," *IEEE Trans. Microwave Theory Tech.*, **MTT-19**, 187 (1971).
Tuntomo, A., C. L. Tien, and S. H. Park, "Internal Distribution of Radiant Absorption in a Spherical Particle," *J. Heat Transfer*, **113**, 407 (1991).
Watson, G. N., *A Treatise on the Theory of Bessel Functions*, Cambridge at the University Press, London England, p. 132 (1966).
Weil, C. M., "Absorption Characteristics of Multilayered Sphere Models Exposed to UHF/Microwave Radiation," *IEEE Trans. Biomed. Eng.*, **BME-22**, 468 (1975).

Appendix

Average power for TM^z polarization: Derivation for Eq. 11

$$P_{\epsilon}^{tm} = \frac{1}{\pi}\int_{\rho=0}^{1}\int_{\phi=0}^{2\pi} uu^*\,\rho\,d\rho\,d\phi. \tag{A1}$$

Substituting

$$u = \sum_{n=0}^{\infty} b_n J_n(\gamma\rho)\cos n\phi, \tag{A2}$$

where $b_n = a_n/E_0$, $\gamma = kR$, and $\rho = r/R$ into Eq. A1,

$$P_c^{tm} = \frac{1}{\pi}\sum_{m=0}^{\infty}\sum_{n=0}^{\infty} b_m b_n^* \int_0^1 \rho J_m(\gamma\rho)J_n(\gamma^*\rho)\,d\rho \times \int_{\phi=0}^{2\pi}\cos m\phi\cos n\phi\,d\phi. \tag{A3}$$

Using the orthogonality of $\cos n\phi$, $0 \le \phi \le 2\pi$, Eq. A3 reduces to Eq. 11,

$$P_c^{tm} = \sum_{n=0}^{\infty}\delta_n b_n I_{n,n}, \tag{A4}$$

where

$$\delta_n = \begin{cases} 2, & n=0; \\ 1, & \text{otherwise}, \end{cases} \qquad b_n = \frac{|a_n|^2}{E_0^2}.$$

Average power for TE^z polarization: Derivation for Eq. 18

$$P_c^{te} = \frac{1}{\pi}\int_{\rho=0}^{1}\int_{\phi=0}^{2\pi}[u_\phi u_\phi^* + u_\rho u_\rho^*]\,\rho\,d\rho\,d\phi. \tag{A5}$$

Using Eqs. 13, 15, 16, and

$$\frac{dJ_n(\gamma\rho)}{d\rho} = -\gamma J_{n+1}(\gamma\rho) + \frac{n}{\rho}J_n(\gamma\rho), \tag{A6}$$

the expressions for

$$u_\phi = \tau\sum_{n=0}^{\infty} d_n\left[\frac{n}{\rho}J_n(\gamma\rho) - \gamma J_{n+1}(\gamma\rho)\right]\cos n\phi \tag{A7}$$

and

$$u_\rho = \frac{\tau}{\rho}\sum_{n=0}^{\infty} n\,d_n J_n(\gamma\rho)\sin n\phi, \tag{A8}$$

where $u_\phi = E_\phi/E_0$, $u_\rho = E_\rho/E_0$, $\tau = c/i\omega(\kappa' + i\kappa'')\,R$, and $d_n = c_n/H_0$. Substituting Eqs. A7 and A8 into Eq. A5 and using the orthogonality of $\cos n\phi$ and $\sin n\phi$; $0 \le \phi \le 2\pi$

$$\begin{aligned} P_c^{te} = {} & 2|\tau|^2|d_0|^2|\gamma|^2\int_0^1 J_1(\gamma\rho)J_1(\gamma^*\rho)\,\rho\,d\rho \\ & + \sum_{n=1}^{\infty}|\tau|^2|d_n|^2\int_0^1\left[2\left(\frac{n}{\rho}\right)^2 J_n(\gamma\rho)J_n(\gamma^*\rho)\right. \\ & - \frac{n}{\rho}\gamma^* J_n(\gamma\rho)J_{n+1}(\gamma^*\rho) - \frac{\gamma n}{\rho}J_{n+1}(\gamma\rho)J_n(\gamma^*\rho) \\ & \left. + \gamma\gamma^* J_{n+1}(\gamma\rho)J_{n+1}(\gamma^*\rho)\right]\rho\,d\rho. \end{aligned} \tag{A9}$$

Replacing J_n using

$$\frac{2n}{\gamma\rho}J_n(\gamma\rho) = J_{n+1}(\gamma\rho) + J_{n-1}(\gamma\rho), \tag{A10}$$

the second integrand in Eq. A9 can be further simplified and

$$P_c^{te} = 2|\tau|^2|d_0|^2|\gamma|^2 I_{1,1} + \frac{1}{2}\sum_{n=1}^{\infty}|\tau|^2|d_n|^2|\gamma|^2[I_{n+1,n+1} + I_{n-1,n-1}]. \tag{A11}$$

Using the expressions for τ, d_n, and γ, Eq. A11 reduces to Eq. 18,

$$P_c^{te} = 2d_0 I_{1,1} + \frac{1}{2}\sum_{n=1}^{\infty} d_n[I_{n+1,n+1} + I_{n-1,n-1}], \tag{A12}$$

where

$$d_n = \frac{|c_n|^2}{H_0^2\sqrt{\kappa'^2 + \kappa''^2}} \qquad n = 0, \ldots, \infty.$$

Manuscript received Jan. 25, 1996, and revision received Sept. 6, 1996.